Ru_xSe_y/C Electrodes for Oxygen Reduction—A Reverse Microemulsion Method of Fabrication of Electrode Material

Ch. Venkateswara Rao and B. Viswanathan*

National Centre for Catalysis Research, Department of Chemistry, Indian Institute of Technology Madras, Chennai 600 036, India

Received: July 15, 2007; In Final Form: August 20, 2007

A reverse microemulsion procedure has been adopted for the preparation of 20 wt % Ru_xSe_y/C (where $x = 1$ and $y = 0-1$). This system has been examined for electrochemical oxygen reduction activity. The measured oxygen reduction activity was comparable with that of commercial Pt/C (E-TEK). The activity is due to stabilization of Ru active sites by Se against blocking as a result of (hydr)oxide formation.

1. Introduction

The cathodic oxygen reduction reaction (ORR) has technological importance in the development of electrochemical power devices like fuel cells and metal−air batteries. This reaction has been studied over the years because of its fundamental complexity, sensitivity to the electrode surface, and sluggish kinetics. Especially in the low-temperature fuel cells (PEMFC and DMFC), it usually contributes considerably to the overpotential (≥300 mV), and therefore results in a low efficiency in the functioning electrochemical devices.[1,2] An extremely active electrocatalyst is needed to reduce the overpotential. To date, the most promising electrocatalyst for oxygen reduction is Pt supported on carbon. Even though it has been commercially exploited, this system has some drawbacks. Those are the formation of −OH species at +0.8 V vs NHE which will hinder the reduction of oxygen, formation of poisoning intermediate species like H_2O_2, expense, and ralatively low abundance of Pt in nature.[3,4] In recent years, there has been significant activity in the development of less expensive non-noble metal-based electrocatalysts which will exhibit both activity and stability similar to that of Pt. Carbon-supported Ru_xSe_y catalysts constitute one class of materials that show activity for oxygen reduction.[5,6] Numerous electrochemical investigations have proven that oxygen reduction occurs on Ru_xSe_y catalysts predominantly via a four-electron reduction path with a negligible amount of hydrogen peroxide intermediate compared to the Pt catalysts.[7−10]

Many methods have been reported on their preparation, including a chemical precipitation method,[11,12] $NaBH_4$ reduction method,[13] impregnation method,[14] colloidal method,[15] and decomposition of organometallic precursors.[12] However, these preparation methods result in difficulties of controlling chemical composition and particle size regardless of metal content. Trapp et al.[11] proposed a low-temperature chemical precipitation method by refluxing metal carbonyls and the corresponding chalcogen in an organic solvent such as xylene or 1,2-dichlorobenzene in an Ar atmosphere. The reaction products consist of nanoscale Ru metals and octahedral clusters of Ru, which contain carbon in the center, surrounded by carbonyl groups. However, because this method involved some complex chemical reactions, a mixture containing several polynuclear compounds with amorphous structures could be produced, depending on the synthesis temperature. It was difficult to separate and characterize these mixtures by traditional chemical methods due to their poor solubility, which was probably one of the drawbacks of this synthesis method. Another disadvantage of this method could be that the yield of the final product was 40−60%. Reeve et al.[12] also carried out the same synthesis using Ru-based electrocatalysts for oxygen reduction. But the activity of the synthesized catalysts is low compared to that of Pt. Recently, Stephen and Campbell[13] disclosed an environment-friendly aqueous method for preparing active catalysts such as Ru_xSe by eliminating the carbonyl precursors and toxic solvents like xylene. In this method, the stoichiometric amounts of active carbon, ruthenium(III) chloride, and selenium dioxide were taken in a water/propanol solvent and stirred at 353 K for 1 h. The resulting mixed solution was then allowed to cool at room temperature. An aqueous solution of NaOH containing $NaBH_4$ was then added to the solution to carry out the chemical reduction reaction. In this way, a carbon-supported catalyst, which has a chemical formula of Ru_xSe, was produced. They claimed that the electrocatalytic ORR activity of prepared catalysts was very close to that of carbon-supported platinum catalysts. Even then the onset potential is 100 mV less than that of commercial Pt/C catalyst. Hilgendorff et al.[14] attempted to synthesize Ru_xSe_y by an impregnation process. One possible drawback of this method is that the temperature used to sinter the catalyst particles is relatively high, which could reduce the catalyst active surface area. In this process, a solution of ruthenium oxalate or carbonyl complex was mixed with a carbon support to form a slurry, which was then dried to remove the solvent. The formed solid was then heated to decompose the salt, in order to produce the desired form of the solid carbon−Ru salt. For selenium incorporation, the solid was dispersed in a solution containing H_2SeO_3. After the chemical reaction between the carbon−Ru salt and H_2SeO_3, a Ru_xSe_y catalyst was produced. The low-temperature chemical precipitation method described has the advantage of allowing the reaction performed in a solution to form bimetallic catalysts at low temperature, and the prepared catalysts normally have a higher active area. However, this method was limited to those reactants which have similar precipitation chemistries or properties, which are easily reduced chemically to metals. In order to minimize this limitation, Tributsch et al.[15] followed the colloidal method

* Corresponding author. E-mail: bvnathan@iitm.ac.in.

10.1021/jp075520w CCC: $37.00
Published on Web 00/00/0000 PAGE EST: 5.9

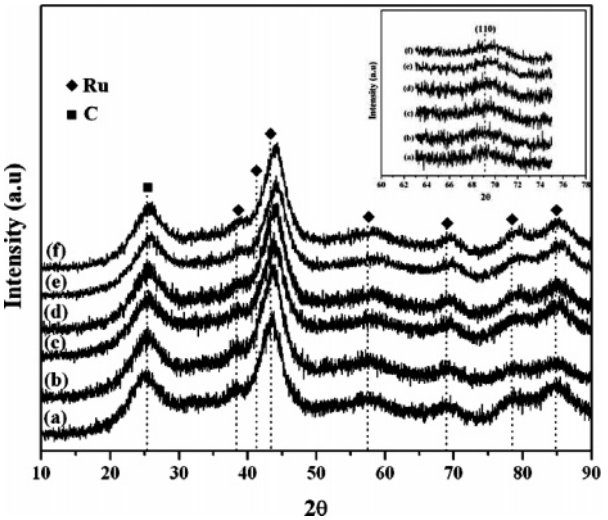

Figure 1. Powder X-ray diffraction patterns of as-synthesized Ru_x-Se_y/CDX975 catalysts: (a) Ru/CDX975, (b) $Ru_1Se_{0.2}$/CDX975, (c) Ru_1-$Se_{0.4}$/CDX975, (d) $Ru_1Se_{0.6}$/CDX975, (e) $Ru_1Se_{0.8}$/CDX975, and (f) Ru_1Se_1/CDX975 (inset shows the slow-scan XRD spectra for the (110) peak of Ru_xSe_y/CDX975 catalysts).

described by Bonnemann et al.[17] in 1991. But the reproducibility was relatively low. The first step for the catalyst synthesis was to make colloidal Ru nanoparticles through $RuCl_3$ reduction in a solution of tetrahydrofuran (THF) containing $N(C_8H_{17})_4BEt_3H$, followed by the addition of absolute ethanol. After that, the mixture was centrifuged (4500 rpm, 15 min) to obtain the solid powder. After the incorporation of selenium, $Ru_xSe_yO_z$ nanoparticles were prepared. The produced catalyst was tested for O_2 reduction, and a fairly high electrocatalytic activity was observed. The high catalytic activity has been attributed to its large surface area, narrow particle size distribution, and ability to prevent particle aggregation. All the methods described above involve difficulty in the control of composition. As a result, various authors obtained Ru_xSe_y catalysts of different Ru and Se compositions with different sizes. So the oxygen reduction activities obtained were not comparable. Recently, Colmenares et al.[9] synthesized Se-modified Ru/C catalysts of controllable compositions by a two-step process: synthesis of Ru/C via a borate route followed by adding controllable amounts of selenium via reductive annealing of the H_2SeO_3-impregnated catalysts at 200 °C in a H_2 gas flow. This method results in Ru_xSe_y/C catalysts with a mean Ru particle diameter of 4 nm with varying amounts of Se and a small amount of oxygen content. Even though they were able to control the composition, paticle size was not the same in all the catalysts. The results obtained by various authors were encouraging, but the ORR activity was not comparable with that of commercial Pt/C. All the electrochemical studies indicate that there is an optimum Ru/Se composition for the maximum ORR activity.

In the past few years, the reverse microemulsion method (RME) has been employed as a suitable method to generate metal colloids and/or clusters on the nanoscale with greater uniformity and controllable composition.[18,19] Reverse micellar solutions are transparent, isotropic, thermodynamically stable water-in-oil microemulsions with nanosized water droplets which are dispersed in a continuous oil phase and stabilized by surfactant molecules at the water/oil interface. The surfactant-stabilized water pools not only act as nanoreactors for processing reactions but also inhibit the excess aggregation of particles because the surfactants could adsorb on the particle surface when the particle size approaches that of the water pool. Consequently, the particles obtained in such a medium are generally very fine and uniform. A number of nanoparticle systems have been prepared in reverse micelles, including metals,[20−22] metal oxides,[23] metal sulfides and selenides,[24,25] metal borides,[26] and organic polymers.[27] However, the preparation of Ru_xSe_y nanoparticles in reverse micelles has not been reported and exploited for oxygen reduction measurements.

In the present study, we have synthesized similar-sized Ru_x-Se_y/C ($x = 1$ and $y = 0-1$) catalysts with controllable composition by a simple and reproducible RME method at room temperature. The resultant catalysts were characterized by X-ray diffraction (XRD), scanning electron microscopy (SEM), transmission electron microscopy (TEM), and energy-dispersive X-ray analysis (EDX). The as-synthesized catalysts were investigated for oxygen reduction and compared with that of commercial Pt/C (E-TEK).

2. Experimental Section

Ruthenium(III) chloride and selenous acid from Sigma-Aldrich, AOT from Acros Organics, sodium borohydride from Merck, and heptane from Fisher Chemicals were used as received. Water purified by a Milli-Q water purification system was used through out the experimental work. Carbon black (CDX975, received from Columbian Chemicals Company) with a specific surface area (BET) of ~300 $m^2\ g^{-1}$ was used as the support for all catalysts.

2.1. Synthesis of 20 wt % Ru_xSe_y/Carbon Black Catalysts. Carbon-supported Ru_xSe_y catalysts (where $x = 1$ and $y = 0-1$) with a metal(s) loading of 20 wt % were prepared by the reverse microemulsion method with the use of sodium bis(2-ethylhexyl) sulfosuccinate (AOT) as the surfactant and heptane as the oil phase. Aqueous solutions of $RuCl_3$, H_2SeO_3, and $NaBH_4$ were used to form the reverse micelle. The size of the particles was controlled by adjusting the molar ratio of surfactant to water ($W = [H_2O]$:[AOT]). Microemulsion 1 was prepared by mixing required amounts of $RuCl_3$, selenous acid, AOT, deionized water, and heptane under constant stirring followed by ultrasonication for 20 min. Microemulsion 2 was prepared by mixing sodium borohydride with small amount of NaOH, AOT, deionized water, and heptane under constant stirring followed by ultrasonication for 20 min. In both microemulsions, the molar ratio of water to AOT was kept at 10:1. Microemulsions 1 and 2 were then mixed together and ultrasonicated for 2 h. Subsequently, an appropriate amount of carbon (CDX975) was added to the mixture to give a metal(s)/C weight ratio of 20:80. The resultant slurry was kept under constant stirring for 2 h, filtered, washed with acetone and deionized water, and dried in an air oven at 348 K for 2 h.

2.2. Characterization Techniques. X-ray diffraction (XRD), scanning electron microscopy (SEM) and transmission electron microscopy (TEM) were used to identify the structure and phase identification, morphology, and particle size, respectively. XRD measurements were performed on a Rigaku Miniflex X-ray diffractometer using a Cu Kα source operated at 30 keV at a scan rate of 0.05° s^{-1} over the 2θ range of 10°−90°. For particle size measurements, XRD spectra were recorded in the 2θ range of 63−75° at a scan rate of 0.02° s^{-1}. The average sizes of metal crystallites were calculated using a Scherrer formula from a fwhm of (110) diffraction line, which for all samples does not overlap with other lines. Transmission electron microscope (TEM) images were obtained by using a high-resolution JEOL 2010 TEM system operated with an accelerating voltage 200 kV. The sample for TEM analysis was prepared by placing a drop of dispersed catalyst onto the carbon-coated copper grid and drying it in air at room temperature. A scanning electron

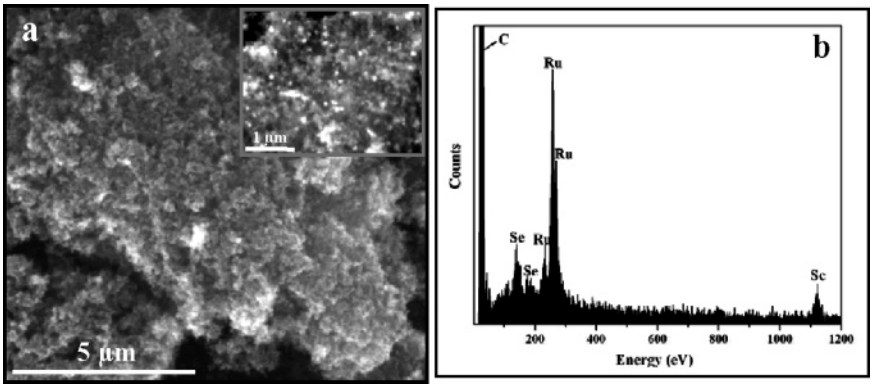

Figure 2. (a) SEM image (inset shows the high magnification image) and (b) EDX spectrum of $Ru_1Se_{0.6}$/CDX975.

TABLE 1: Elemental Composition, Se/Ru Atomic Ratio, Crystallite Size, Onset Potential for Oxygen Reduction, and ORR Activities of 20 wt % Ru_xSe_y/CDX975 ($x = 1$ and $y = 0-1$) and Commercial 20 wt % Pt/C (E-TEK) Catalysts

catalyst	elemental composition by EDX	Se/Ru atomic ratio	crystallite size from XRD (nm)	onset potential (V) for oxygen reduction	ORR activity at +0.65 V vs NHE (mA/ cm^2)
Ru/CDX975	100:-	0.0	3.0	+850	1.3
$Ru_1Se_{0.2}$/ CDX975	87.7:12.3	0.18	3.0	+875	2.1
$Ru_1Se_{0.4}$/ CDX975	76.6:23.4	0.38	3.1	+890	3.0
$Ru_1Se_{0.6}$/ CDX975	68.5:31.5	0.59	3.1	+905	4.2
$Ru_1Se_{0.8}$/ CDX975	62.2:37.8	0.78	3.1	+885	1.6
Ru_1Se_1/ CDX975	56.2:43.8	1.00	3.1	+870	1.4
Pt/C (E-TEK)				+930	4.0

microscope with EDX (FEI, Model: Quanta 200) was used to observe the surface morphology and composition of the catalysts.

2.3. Electrochemical Measurements. Activity of the as-synthesized Ru_xSe_y/ CDX975 (where $x = 1$ and $y = 0-1$) and commercial Pt/C catalysts was determined by cyclic voltammetry using a potentiostat (BAS 100 electrochemical analyzer). All experiments were performed at room temperature in a conventional one-compartment electrochemical glass cell assembled with a glassy carbon (GC) disk as the working electrode, Ag/AgCl, 3.5 M KCl (+0.205 V vs NHE) as the reference electrode, and Pt foil as the counter electrode, respectively. Oxygen-saturated 0.5 M H_2SO_4 was the electrolyte. The electrode was fabricated as follows: 5 mg of the catalyst, 0.5 mL of diluted Nafion solution (Aldrich, 5 wt % in 15−20% water/low aliphatic alcohols), and 0.5 mL of isopropyl alcohol were ultrasonically blended for 20 min. A GC disk (0.07 cm^2) was polished to a mirror finish with 0.05 μm alumina suspensions before each experiment and served as an underlying substrate of the working electrode. An aliquot of 5 μL of catalyst suspension was pipetted onto the mirror polished glassy carbon substrate, leading to a metal loading of 70 μg_{metal} cm^{-2}, and dried in flowing argon at room temperature. After preparation, the electrodes were immersed in deaerated 0.5 M H_2SO_4. Then the cyclic voltamograms were recorded between +0.0 and +1.0 V vs NHE at a scan rate of 20 mV/s. For oxygen reduction measurements, linear sweep voltammograms (LSVs) were recorded between +0.2 and +1.2 V vs NHE at a scan rate of 5 mV/s in both Ar- and O_2-saturated 0.5 M H_2SO_4.Oxygen reduction activity was calculated by taking the difference in activity at +0.65 V vs NHE in Ar- and O_2- saturated 0.5 M H_2SO_4. Current densities are normalized to the geometric area of the glassy carbon substrate (0.07 cm^2) in the following text.

3. Results and Discussion

3.1. XRD Analysis. Figure 1 shows the powder X-ray diffraction patterns of the Ru_xSe_y/CDX975 catalysts. All the as-synthesized Ru_xSe_y/CDX975 catalysts show peaks at 2θ values around 38°, 42°, 44°, 58°, 69°, 78°, and 85° corresponding to the (100), (002), (101), (102), (110), (103), and (112) planes of ruthenium, respectively. These characteristic peaks can be assigned to *hcp* ruthenium. The positions and intensities of *hcp* ruthenium diffraction lines are in good agreement with those of the JCPDS powder diffraction data file no. 89-4903. The broad peaks indicate that the particles were in nanocrystalline range. With an increase of the Se/Ru atomic ratio, Ru diffraction lines shift slightly to higher 2θ values with respect to the corresponding peaks in the Ru/CDX975 catalyst (obeying Vegard's law), indicating the solubility of Se in Ru lattice. The broad diffraction peak observed at around $2\theta = 25°$ corresponds to the (002) plane diffraction of the hexagonal structure of the carbon support. The average particle size for the Ru_xSe_y/ CDX975 catalysts was calculated from broadening of the (110) diffraction peak (shown as an inset in Figure 1) using Scherrer's equation: $L = (0.9\lambda)/(\beta_{1/2} \cos \theta)$, where λ is the wavelength of the X-ray (1.5406 Å), θ is the angle at the position of the peak maximum, and $\beta_{1/2}$ is the width (in radians) of the diffraction peak at half-height.[8] The obtained results are shown in Table 1. The average particle size of metallic nanoparticles in 20 wt % Ru_xSe_y/CDX975 catalysts are estimated to be around 3.0 nm.

3.2. SEM, EDX, and TEM Analysis. Figure 2 shows the scanning electron microscopic (SEM) image and the corresponding EDX spectrum of $Ru_1Se_{0.6}$/CDX975 catalyst. Agglomeration of spherical-shaped carbon with metallic particles can be seen from the SEM image (Figure 2a). Elemental analysis performed by EDX confirms the presence of Ru, Se, C, and a very small quantity of oxygen (Figure 2b). The calculated elemental composition (Ru/Se) in $Ru_1Se_{0.6}$/CDX975 is about (wt %) 68.5:31.5, corresponding to a Se/Ru atomic ratio of 0.59. Similarly we have analyzed the other catalysts of different Ru and Se composition. For each molar ratio of Ru/Se, some regions were chosen randomly to analyze the composition by EDX attached to a SEM. The results are given in Table 1. The slight deviation of composition among different particles at each $[RuCl_3]/[H_2SeO_3]$ ratio might result from the detection errors. The deviation could be due to the detection errors and the fact

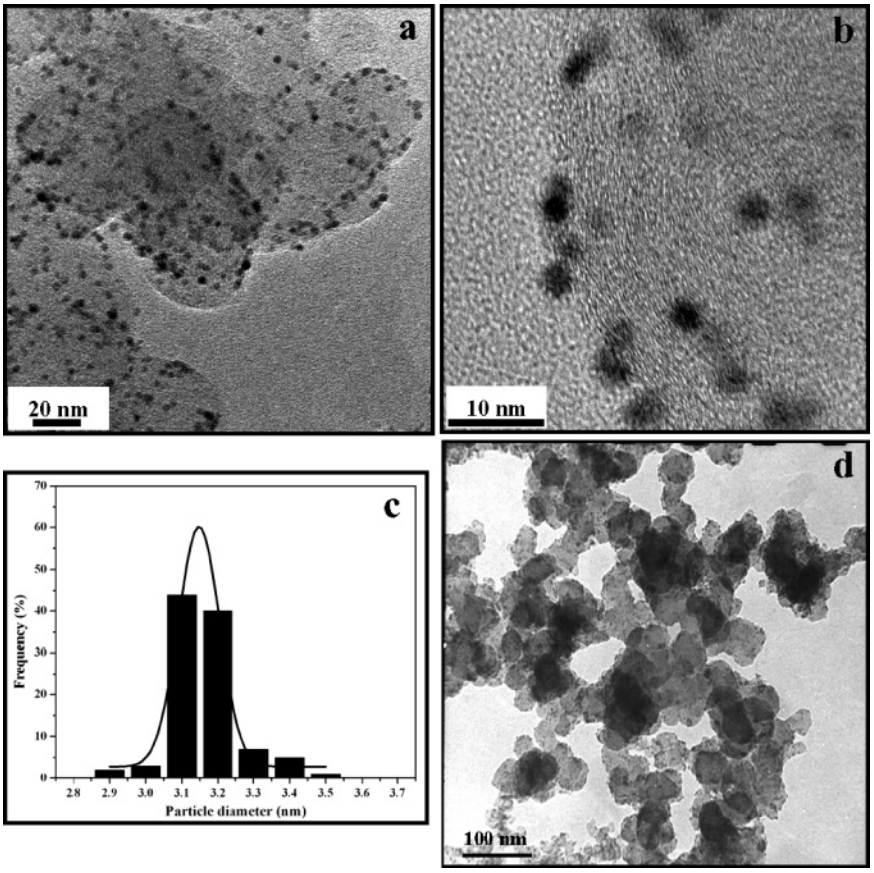

Figure 3. TEM images of (a) $Ru_1Se_{0.6}$/CDX975 at low magnification and (b) $Ru_1Se_{0.6}$/CDX975 at high magnification. Histograms of (c) $Ru_1Se_{0.6}$ particles on CDX975 and (d) commercial Pt/C (E-TEK).

that fewer regions were chosen for analysis. In addition, it was observed that the average compositions were roughly in agreement with those of the initial metal salt solutions.

Figure 3 represents the TEM images of the as-synthesized $Ru_1Se_{0.6}$/CDX975 and commercial Pt/C catalysts. Well-dispersed, uniform-size, and spherical-shaped metallic nanoparticles with an average size of 3.1 nm on the carbon support can be seen from both the low- and high-magnification TEM images (Figure 3a,b). The average crystallite size calculated from the XRD peak width was found to be consistent with those obtained from the TEM result. Figure 3c shows the narrow size distribution of $Ru_1Se_{0.6}$ metallic nanoparticles on a carbon support. For comparison, a TEM image of commercial Pt/C is also shown in Figure 3d. The average particle size of Pt in the case of the commercial catalyst is 3.7 nm, which is in good agreement with the literature report.[7]

3.3. Electrochemical Performances. Linear sweep voltammetry (LSV) was performed to measure the oxygen reduction activity of as-synthesized Ru_xSe_y/CDX975 and commercial Pt/C (E-TEK) catalysts in Ar- and O_2-saturated 0.5 M H_2SO_4. The obtained voltammograms are shown in Figure 4. It is clear that the electrode prepared by using as-synthesized $Ru_1Se_{0.6}$/CDX975 shows higher oxygen reduction activity than other Ru catalysts. A high oxygen reduction current is paramount for an efficient electrochemical power device.

Figure 4 indicates that the ORR kinetics is not the same on all the catalysts. Oxygen reduction is facile in the case of Se/Ru atomic ratios of 0.2, 0.4, and 0.6 compared to the Se/Ru atomic ratios of 0, 0.8, and 1.0. In the case of Ru_xSe_y/C catalysts with $x = 1$ and $y = 0.2-0.6$, ORR is diffusion-controlled at potentials below +0.6 V and diffusion- and kinetics-controlled

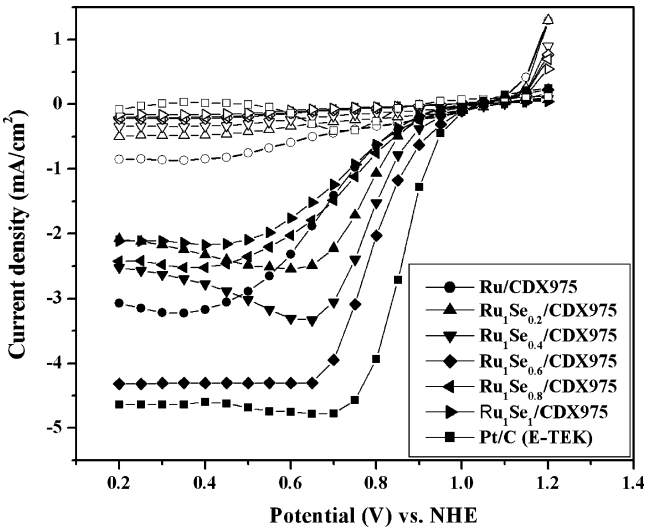

Figure 4. Linear sweep voltammograms (LSVs) of O_2 reduction on 20 wt % Ru_xSe_y/CDX975 and commercial Pt/C (E-TEK) catalysts in 0.5 H_2SO_4; scan rate: 5 mV s^{-1}. (Empty and full symbols correspond to the LSVs in Ar- and O_2-saturated 0.5 M H_2SO_4, respectively).

in the potential region between +0.6 and +0.95 V vs NHE. In the case of Ru_xSe_y/C catalysts with $x = 1$ and $y = 0$, 0.8, and 1.0, ORR is diffusion-controlled at potentials below +0.4 V and diffusion- and kinetics-control in the potential region between +0.4 and +0.9 V vs NHE. The reason for the different curve shapes for Ru_xSe_y/C catalysts with different Se/Ru atomic ratios may be due to the variation of geometric and electronic factors like the Ru−Ru interatomic distance, Ru−Se distance,

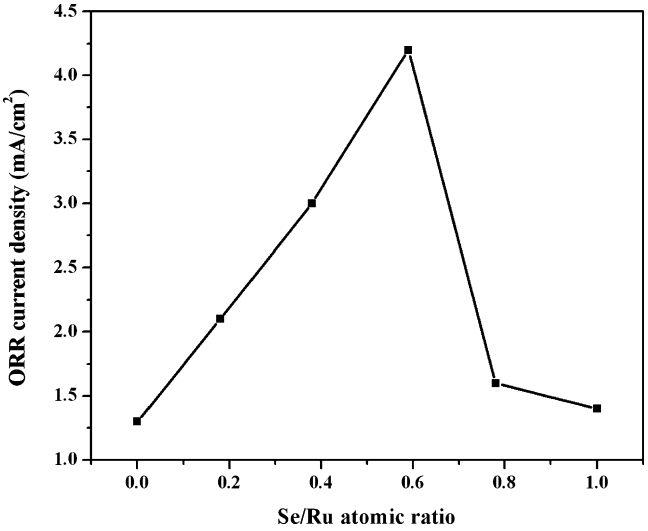

Figure 5. Se/Ru atomic ratio vs ORR current density of as-synthesized Ru_xSe_y/CDX975 catalysts.

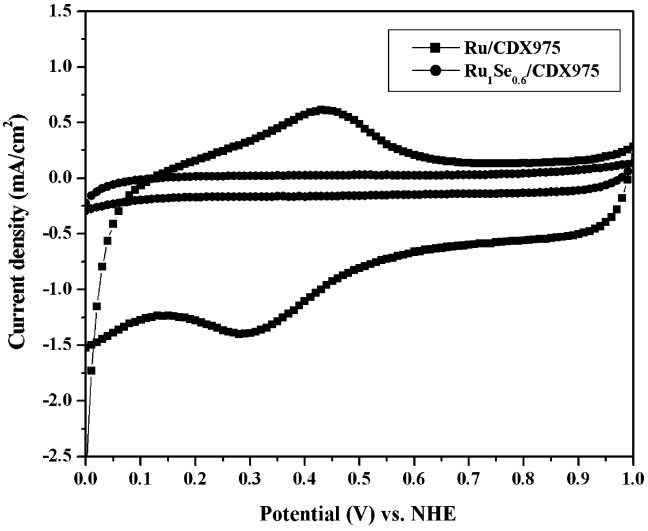

Figure 6. Cyclic voltammograms (CVs) of (■) Ru/CDX975 and (●) $Ru_1Se_{0.6}$/CDX975 catalysts in Ar-saturated 0.5 H_2SO_4; scan rate: 20 mV s^{-1}.

Ru coordination number, and binding capacity of Se toward Ru active species.[8,10] For all the Ru-based catalysts, when the potential was swept from +1.2 to +0.2 V vs NHE, a single oxygen reduction peak is observed in the potential region of about 1.0−0.4 V. This corresponds with the four-electron reduction pathway of O_2 to H_2O.[7,9,10] The steep increase in peak current at +0.65 V indicates the facile kinetics of ORR. At the lower amounts of Se/Ru atomic ratio of 0.2, the formation of −OH species was inhibited to some extent compared to the Ru/CDX975. As a result, both the onset potential and activity were increased. This is more prominent in the case of a Se/Ru atomic ratio of 0.4 and 0.6. At a Se/Ru atomic ratio of 0.6, the formation of −OH species on the Ru surface was completely inhibited. At this composition, the geometric and electronic factors/ Ru−Ru interatomic distance may be optimum so that it favors the dissociation of the oxygen molecule and facile transfer of electrons; consequently, there is a steep increase of oxygen reduction peak current. At Se contents beyond 0.6, even though the formation of −OH species was inhibited, the Ru active species were blocked by the presence of Se. As a result, the oxygen reduction was started at potentials of +0.85 V vs NHE and complete reduction took place at potentials of +0.4 V vs NHE.

The obtained oxygen reduction current densities normalized to the geometric area are plotted as a function of the Se/Ru atomic ratio in Figure 5. It shows that the current density exhibits a maximum for the $Ru_1Se_{0.6}$/C catalyst. Further increase in Se content results in a decrease of the ORR activity, which however still exceeds the catalytic activity of the Ru/C catalyst. Recently Fiechter et al.[10] also observed the higher selectivity (98−99%) for oxygen reduction to water at moderate Se loadings (y = 0.3−0.6) under cathode-relevant reaction conditions. Moreover, oxygen reduction activity of the as-synthesized $Ru_1Se_{0.6}$/CDX975 (4.2 mA cm^{-2}) was comparable to that of the commercial Pt/C (E-TEK) catalyst (4.0 mA cm^{-2}).

Figure 6 represents the cyclic voltammograms (CVs) of Ru/CDX975 and $Ru_1Se_{0.6}$/CDX975 in deaerated 0.5 M H_2SO_4. It reveals the commencement of oxide/hydroxide species on the Ru surface at potentials of +0.25 V. The cathodic broad counter peak between +0.15 and +0.45 V can be thus attributed to the surface oxide/hydroxide reduction, and the negative shift of oxide/hydroxide reduction suggests an increased irreversibility of the surface oxidation.[28,29] It is well-known in the literature that with increasing OH_{ad} formation/surface oxidation, diminishing the ORR activity[7,8] and also it has been shown that a pure oxide such as RuO_2 at the metallic ruthenium surface, which would be encountered at potentials of practical oxygen electrodes (0.7−0.9 V vs NHE) is inactive toward oxygen reduction.[30] In the case of $Ru_1Se_{0.6}$/CDX975 catalyst, the formation of oxide/hydroxide species formation/reduction was not observed. It indicates that the presence of Se is inhibiting the electrochemical oxidation of Ru and stabilizing the Ru active centers in such a way that it exhibited high ORR activity. Recent studies have shown that similar ORR enhancement can be reached by modifying Ru nanoparticles with Se.[7−10] Despite numerous investigations on the structure and electrochemical properties of Ru_xSe_y cluster materials,[31−35] the role of Se in the enhancement of the catalytic activity is not yet fully understood. Our studies indicate that the presence of selenium in the prepared catalysts is stabilizing the Ru active centers upon electrochemical oxidation and the optimum selenium content is 0.6. At this optimum Se/Ru atomic ratio, there may be a facile interaction between the metal d-orbitals and adsorbate valence states so that electron transfer takes place from the metal d-orbital to the antibonding $2\pi^*$-orbital of molecular oxygen.

In comparison with Pt/C catalyst, the kinetically controlled region of the ORR is shifted negatively by ∼100 mV on the Ru/CDX975 catalyst. This shift of the ORR is attributed to the onset of OH_{ad} formation and Ru surface oxidation at lower potentials (+0.3 V vs NHE) than on the Pt electrode (+0.68 V vs NHE). In the case of Ru_xSe_y/CDX975 catalysts, a noticeable shift of the ORR in the kinetic region to more positive values is observed for moderate amounts of Se (0.4−0.6) to the Ru. For higher Se/Ru ratios, the onset of the ORR is shifted back to lower potentials. Qualitatively similar shifts were also observed in potentiodynamic R(R)DE measurements performed by Zaikovskii et al.[8]

All these measurements indicate that the $Ru_1Se_{0.6}$/CDX975 catalyst shows an ORR activity significantly comparable with that of the Pt/C catalyst in the technically relevant potential regime between +0.6 and +0.8 V. But the overpotential for the O_2 reduction is about 20−30 mV higher than for the Pt/C catalyst.

Long-term stability of the catalysts is important for practical applications. The current density−time plot of as-synthesized

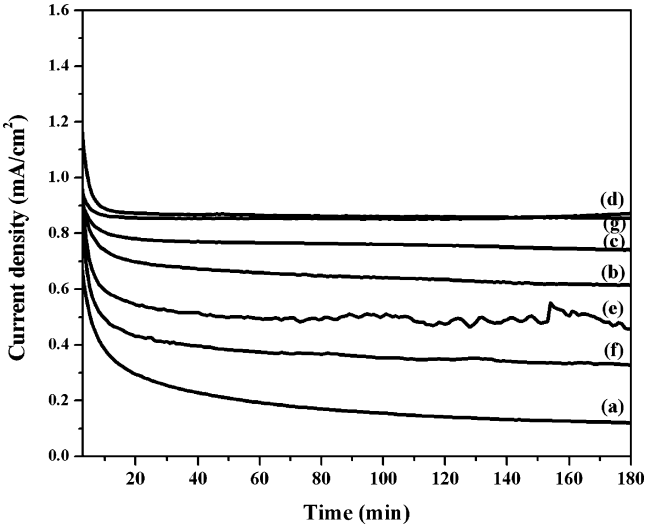

Figure 7. Current density vs time curves of as-synthesized 20 wt % Ru_xSe_y/CDX975 catalysts: (a) Ru/CDX975, (b) $Ru_1Se_{0.2}$/CDX975, (c) $Ru_1Se_{0.4}$/CDX975, (d) $Ru_1Se_{0.6}$/CDX975, (e) $Ru_1Se_{0.8}$/CDX975, (f) Ru_1Se_1/CDX975, and (g) commercial Pt/C (E-TEK) measured in oxygen-saturated 0.5 M H_2SO_4 at +0.65 V vs NHE.

20 wt % Ru_xSe_y/CDX975 and commercial 20 wt % Pt/C catalysts in oxygen-saturated 0.5 M H_2SO_4 at +0.65 V vs NHE is shown in Figure 7. It shows that the performance of Ru_xSe_y/CDX975 catalysts is better than that of Ru/CDX975. This is due to the inhibition of (hydr)oxide formation and stabilization of Ru active centers by means of Se additive. Among all the carbon-supported Ru_xSe_y catalysts, $Ru_1Se_{0.6}$/CDX975 exhibited high performance and it is quite similar to that of the commercial Pt/C (E-TEK) catalyst. The increasing order of stability of electrodes is as follows: Ru/CDX975 < Ru_1Se_1/CDX975 < $Ru_1Se_{0.8}$/CDX975 < $Ru_1Se_{0.2}$/CDX975 < $Ru_1Se_{0.4}$/CDX975 < $Ru_1Se_{0.6}$/CDX975 ≈ commercial Pt/C (E-TEK).

4. Conclusions

The reverse microemulsion method (RME) has been adopted to synthesize 20 wt % Ru_xSe_y/CDX975 catalysts. XRD measurements indicate the existence of Ru in the *hcp* phase as well as similar particle size (around 3 nm) in all the as-synthesized catalysts. EDX reveals the composition obtained for the as-synthesized catalysts were roughly in agreement with those of the starting metal content. The TEM image of $Ru_1Se_{0.6}$/CDX975 shows the high dispersion of metallic particles on carbon (CDX975) support. Evaluation of a series of Ru_xSe_y/CDX975 catalysts for the O_2 reduction by LSV measurements reveals the improvement of ORR activity by the presence of Se with a maximum activity (geometric area-normalized current density) for the $Ru_1Se_{0.6}$/CDX975 catalyst. The reason for the improved activity is the stabilization of Ru active sites by Se against blocking as a result of (hydr)oxide formation. The comparable ORR activity and stability of $Ru_1Se_{0.6}$/CDX975 with those of commercial Pt/C (E-TEK) catalyst makes it an ideal cathode material for electrochemical power devices.

Acknowledgment. The authors thank the Department of Science and Technology, Government of India, and the Columbian Chemicals Company, USA, for the financial support.

References and Notes

(1) *Fuel cells − Principles and Applications*; Viswanathan, B., Aulice Scibioh, M., Eds.; Universities Press (India) Private Limited, 2006.

(2) Viswanathan, B.; Rao, Ch. Venkateswara; Varadaraju, U. V. *Photo/Electrochemistry & Photobiology in the Environment, Energy and Fuel* **2006**, 43.

(3) Ralph, T. R.; Hogarth, M. P. *Platinum Met. Rev.* **2002**, *46*, 3.

(4) Shukla, A. K.; Raman, R. K. *Annu. Rev. Mater. Res.* **2003**, *33*, 155.

(5) Alonso-Vante, N.; Tributsch, H. *Nature* **1986**, *323*, 431.

(6) Alonso-Vante, N.; Bogdanoff, P.; Tributsch, H. *J. Catal.* **2000**, *190*, 240.

(7) Colmenares, L.; Jusys, Z.; Behm, R. J. *Langmuir* **2006**, *22*, 10437.

(8) Zaikovskii, V. I.; Nagabhushana, K. S.; Kriventsov, V. V.; Loponov, K. N.; Cherepanova, S. V.; Kvon, R. I.; Bonnemann, H.; Kochubey, D. I.; Savinova, E. R. *J. Phys. Chem. B* **2006**, *110*, 6881.

(9) Colmenares, L.; Jusys, Z.; Behm, R. J. *J. Phys. Chem. C* **2007**, *111*, 1273.

(10) Fiechter, S.; Dorbandt, I.; Bogdanoff, P.; Zehl, G.; Schulenburg, H.; Tributsch, H.; Bron, M.; Radnik, J.; Fieber-Erdmann, M. *J. Phys. Chem. C* **2007**, *111*, 477.

(11) Trapp, V.; Christensen, P. A.; Hamnett, A. *J. Chem. Soc., Faraday Trans.* **1996**, *92*, 4311.

(12) Reeve, R. W.; Christensen, P. A.; Hamnett, A.; Haydock, S. A.; Roy, S. C. *J. Electrochem. Soc.* **1998**, *145*, 3463.

(13) Stephen, A. Campbell, U.S. Patent 2004/0096728A1, 2004.

(14) Hilgendorff, M.; Bogdanoff, P.; Bron, M. *Proceedings of the Fuel cell systems of the world renewable energy congress VII*, 2003; Vol. 26.

(15) Tributsch, H.; Bron, M.; Hilgendorff, M.; Schulenburg, H.; Dorbandt, I.; Eyert, V.; Bogdanoff, P.; Fiechter, S. *J. Appl. Electrochem.* **2001**, *31*, 739.

(16) Vogel, W.; Kaghazchi, P.; Jacob, T.; Alonso-Vante, N. *J. Phys. Chem. C* **2007**, *111*, 3908.

(17) Bonnemann, H.; Brijoux, W.; Brinkmann, R.; Dinjus, E.; Fretzen, R.; JouBen, T.; Korall, B. *Angew. Chem.* **1991**, *103*, 1344.

(18) Kim, W.-Y.; Hayashi, H.; Kishida, M.; Nagata, H.; Wakabayashi, K. *Appl. Catal.* **1998**, *169*, 57.

(19) Kishida, M.; Umakoshi, K.; Ishiyama, J.; Nagata, H.; Wakabayashi, K. *Catal. Today* **1996**, *29*, 355.

(20) Chen, D. H.; Wu, S. H. *Chem. Mater.* **2000**, *12*, 1354.

(21) Raghuveer, V.; Ferreira, P. J.; Manthiram, A. *Electrochem. Commun.* **2006**, *8*, 807.

(22) Taleb, A.; Petit, C.; Pileni, M. P. *Chem. Mater.* **1997**, *9*, 950.

(23) Raghuveer, V.; Keshav, Kumar; Viswanathan, B. *Indian J. Eng. Mater. Sci.* **2002**, *9*, 137.

(24) Kortan, A. R.; Hull, R.; Opila, R. L.; Bawendi, M. G.; Steigerwald, M. L.; Carroll, P. J.; Brus, L. E. *J. Am. Chem. Soc.* **1990**, *112*, 1327.

(25) Haram, S. K.; Mahadeshwar, A. R.; Dixit, S. G. *J. Phys. Chem.* **1996**, *100*, 5868.

(26) Nagy, J. *J. Colloids Surf.* **1989**, *35*, 201.

(27) Antonietti, M.; Basten, R.; Lonmann, S. *Macromol. Chem. Phys.* **1995**, *196*, 441.

(28) El-Aziz, A. M.; Kibler, L. A. *Electrochem. Commun.* **2002**, *4*, 866.

(29) Marinkovic, N. S.; Wang, J. X.; Zajonz, H.; Adzic, R. R. *J. Electroanal. Chem.* **2001**, *500*, 388.

(30) Nekrasov, L. N.; Kruscheva, E. I. *Elektrokhimiya* **1967**, *3*, 166.

(31) Solorza-Feria, O.; Ellmer, K.; Giersig, M.; Alonso-Vante, N. *Electrochim. Acta* **1994**, *39*, 1647.

(32) Alonso-Vante, N.; Solorza-Feria, O. *Electrochim. Acta* **1995**, *40*, 567.

(33) Alonso-Vante, N.; Borthen, P.; Fieber-Erdmann, M.; Strehblow, H. H.; Holub-Krappe, E. *Electrochim. Acta* **2000**, *45*, 4227.

(34) Dassenoy, F.; Vogel, W.; Alonso-Vante, N. *J. Phys. Chem. B* **2002**, *106*, 12152.

(35) Le Rhun, V.; Alonso-Vante, N. *J. New Mater. Electrochem. Syst.* **2000**, *3*, 331.